

*Integrating spatial, temporal, and  
magnitude probabilities for medium-  
scale landslide risk analysis in Darjeeling  
Himalayas, India*

**Saibal Ghosh, Cees J. van Westen,  
Emmanuel John M. Carranza & Victor  
G. Jetten**

**Landslides**

Journal of the International Consortium  
on Landslides

ISSN 1612-510X

Landslides

DOI 10.1007/s10346-011-0304-6



**Your article is protected by copyright and all rights are held exclusively by Springer-Verlag. This e-offprint is for personal use only and shall not be self-archived in electronic repositories. If you wish to self-archive your work, please use the accepted author's version for posting to your own website or your institution's repository. You may further deposit the accepted author's version on a funder's repository at a funder's request, provided it is not made publicly available until 12 months after publication.**

Landslides  
 DOI 10.1007/s10346-011-0304-6  
 Received: 30 April 2011  
 Accepted: 10 November 2011  
 © Springer-Verlag 2011

Saibal Ghosh · Cees J. van Westen · Emmanuel John M. Carranza · Victor G. Jetten

## Integrating spatial, temporal, and magnitude probabilities for medium-scale landslide risk analysis in Darjeeling Himalayas, India

**Abstract** Landslide risk assessment is based on spatially integrating landslide hazard with exposed elements-at-risk to determine their vulnerability and to express the expected direct and indirect losses. There are three components that are relevant for expressing landslide hazard: spatial, temporal, and magnitude probabilities. At a medium-scale analysis, this is often done by first deriving a landslide susceptibility map, and to determine the three types of probabilities on the basis of landslide inventories linked to particular triggering events. The determination of spatial, temporal, and magnitude probabilities depend mainly on the availability of sufficiently complete historical records of past landslides, which in general are rare in most countries (e.g., India, etc.). In this paper, we presented an approach to use available historical information on landslide inventories for landslide hazard and risk analysis on a medium scale (1:25,000) in a perennially typical data-scarce environment in Darjeeling Himalayas (India). We demonstrate how the incompleteness in the resulting landslide database influences the various components in the calculation of specific risk of elements-at-risk (e.g., buildings, population, roads, etc.). We incorporate the uncertainties involved in the risk estimation and illustrate the range of expected losses in the form of maximum and minimum loss curves. The study demonstrates that even in data-scarce environments, quantitative landslide risk assessment is a viable option, as long as the uncertainties involved are expressed.

**Keywords** Landslide hazard and risk analysis · Uncertainty · Darjeeling Himalayas · Spatial and temporal probability

### Introduction

Landslides can occur as potential natural hazards causing huge damage to the environment and society leading to loss of lives and resources. Societies that are affected frequently with such damaging landslides need suitable scientific advice to understand the phenomena and develop expertise on the prediction that deals with space, time, and magnitude of such damaging events, so that appropriate mitigative measures can be suitably planned. Accordingly, landslide hazard is defined as the likelihood of a damaging landslide phenomenon of certain magnitude that is expected to occur in a certain period of time and area (Varnes 1984 and UNESCO's IAGC Commission on landslides and other mass movements; Guzzetti et al. 1999). The conventional spatial prediction of landslides or predictive mapping of landslide susceptibility, is therefore, not sufficient enough to predict "when"/"how often" and "how large" the future landslides would be, for which, estimations of frequency and magnitude of such events and integration of those estimates into the susceptibility maps are necessary (van Westen et al. 2006; Guzzetti et al. 2005). There is need to go a step beyond the susceptibility approach and to focus on the estimation of probable losses or risks in order to

be able to properly allocate resources to landslide risk reduction (Fell et al. 2008; Guzzetti 2002; Fell and Hartford 1997).

Quantitative landslide hazard and risk analysis requires the availability of sufficient historical landslide information in order to estimate the spatial, temporal, and magnitude probabilities (Einstein 1997; Cruden 1997; Zêzere et al. 2008; Fell et al. 2008; Malamud et al. 2004; Salvati et al. 2010). However, in most cases, information on past landslides is scarce which acts as a serious deterrent in correctly predicting landslide hazard scenarios and thereby impedes subsequent quantitative risk assessment, especially at mapping scales smaller than say 1:5,000. Therefore, in an area where historic information on past landslides is absent or incomplete, landslide risk assessment is extremely difficult, if not impossible (van Westen et al. 2006). This problem is quite common, especially, in most of the developing countries like India and has therefore, compelled many landslide scientists to rely more on the susceptibility maps to do a qualitative/semi-quantitative landslide hazard and risk assessment (Rautela and Lakhera 2000; Anbalagan and Singh 1996; Kanungo et al. 2008). Moreover in literature, not much research on medium-scale (1:25,000) quantitative landslide hazard and risk analysis in such a data-scarce environment is available, where varying levels of uncertainties that are expected to propagate in quantitative landslide hazard and risk analysis are shown.

In order to address the above issue, this research was undertaken because quantitative estimation of landslide hazard and risk (a) renders a standardized and quantifiable way to express the expected impact of landslides and (b) facilitates a more objective way to allocate or prioritize resources for mitigation by the administrators. This paper thus outlines some suitable and uniform methods of medium-scale landslide hazard and risk assessments that are also applicable to similar data-scarce environments in India and can easily be followed by the scientific organizations in India, engaged in regional landslide mitigation programs.

The hazard and risk analysis enumerated in this paper was undertaken in a landslide-prone terrain around Kurseong town in the Darjeeling district, West Bengal, India, which falls within the fragile fold-thrust-belt of the Eastern Himalayas (Fig. 1; Ghosh and Carranza 2010). The area is characterized by a prominent NE-SW trending ridge in the central part with elevations varying from 236 to 2,189 m and slopes vary from 0° to 84° (Ghosh et al. 2011b). Slopes are gentler on ridge tops but become increasingly steeper downward to the streams (Dutta 1966; Binnie et al. 2007; Burbank et al. 1996). Climate is humid with a long period (June–October) of monsoon-controlled heavy precipitation. Annual precipitation varies between 2,000 and 5,000 mm (Soja and Starkel 2007).

### Landslides and source data sets

Denudational geomorphic processes are predominant in the Himalayas due to the active tectonic processes. It has been

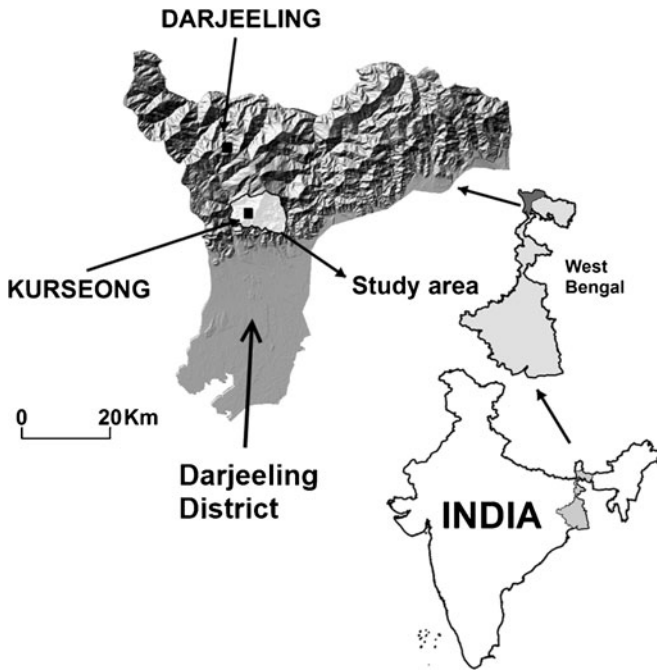


Fig. 1 Location map of the study area

demonstrated by several workers in the adjacent Nepalese Himalayas (Selby 1988; Caine and Mool 1982; Petley et al. 2007) that the high frequency of slope failures in the Eastern Himalayas can be attributed to a very high rate of denudation (i.e., 5–14 mm year<sup>-1</sup>) associated with active tectonic processes

of Himalayan orogeny. Moreover, high rate of precipitation (Soja and Starkel 2007) in the Eastern Himalays accentuates activation/reactivation of innumerable number of landslides in Darjeeling-Sikkim Himalayas (Starkel and Basu 2000). To quantify the impact of such landslides, despite data gaps, we have already attempted to generate event-based landslide inventory maps for the study area (Fig. 2) for triggering events over a 40-year period (1968 to 2007) based on the available source data (e.g., archives, reports, old landslide occurrence maps, high-resolution aerial photos, satellite images, etc.; Ghosh et al. 2011b). The above inventory maps were subsequently used as landslide source data for susceptibility, hazard, and risk analyses.

We also created predictive models of landslide susceptibility to shallow translational rocksliding (Sh\_rs) and debris sliding (Db\_rs) in the study area by empirically selecting and weighting spatial predictors of such landslides through a two-stage methodology: (a) quantifying associations of individual spatial factors with landslides of different types using bivariate analysis to select predictors; and (b) pairwise comparisons of the quantified associations using an analytical hierarchy process to assign predictor weights. We subsequently integrated the weighted spatial predictors through multi-class index overlay to derive the predictive models of landslide susceptibility (Ghosh et al. 2011a). In the present study, we used such predictive maps of landslide susceptibility to rockslides (Sh\_rs) and to debris slides (Db\_rs) to calculate the impacts of each of the landslide types separately for different hazard scenarios.

We collected data from the local village or administrative authorities, municipalities, and census for mapping and characterizing elements-at-risk (focusing on buildings and roads) and demographic data at the level of settlement units (which are the

Fig. 2 Lithology map with landslide occurrences in the study area

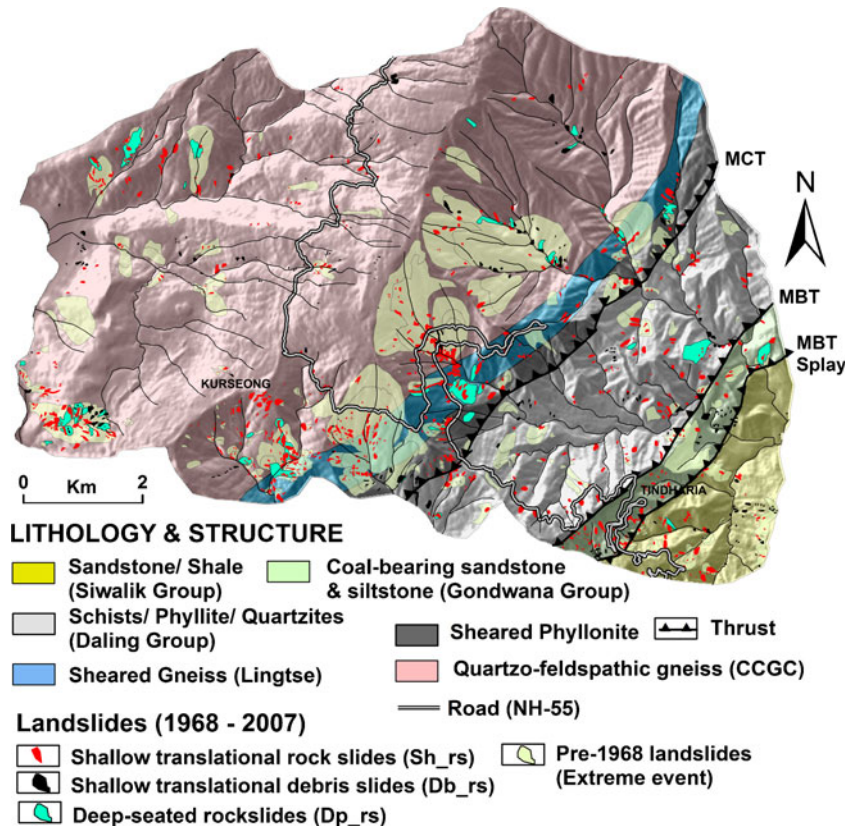


**Table 1** Details of different elements-at-risk used to calculate expected losses

Details of elements-at-risk data	
Number of settlement units (SUs)	236
Total number of buildings	13,736
Density of buildings (maximum)	1.0 (nos./100 m <sup>2</sup> )
Density of buildings (minimum)	0.005 (nos./100 m <sup>2</sup> )
Total number of RCC buildings	1,945
Total number of concrete buildings	5,208
Total number of squatter buildings	6,583
Total population	76,126
Population density (maximum) per SU	18.86 per 100 m <sup>2</sup>
Population density (minimum) per SU	0.051 per 100 m <sup>2</sup>
Population density (average for the entire study area)	0.08 per 100 m <sup>2</sup>
Population density in urban area (average)	2.12 per 100 m <sup>2</sup>
Population density in rural area (average)	0.04 per 100 m <sup>2</sup>
Total length (km) of major roads	162 km

Source: Census of India, 2001 and Rural Household Survey (RHS), 2006

smallest administrative units) for population. For spatial representation of this data in the form of settlement units (hereafter denoted as SU), we first prepared a land-use/land-cover map from high-resolution satellite imagery (5-m resolution IRS P6 MX image of 2004), and combined it with the census blocks and village maps to make a settlement unit map containing 236 SUs (Fig. 3). We obtained information on the number of buildings and population for each village from the reports of a Rural Household Survey (RHS) from 2006, which were integrated with the SU map. Each SU contains attribute information on the total number of buildings, type of dwelling structure and population, and its related demographic details including number of children, employed people, etc. (Fig. 3a and b; Table 1). For areas within the town of Kurseong, we obtained the above information both from the census and municipality records. As this research focuses on medium-scale analysis (1:25,000), the SUs are considered as the basic units for loss estimation. Apart from the settlement units, we also prepared a map of the road network to calculate the likelihood of direct losses along roads in different hazard scenarios (Fig. 3c).

In this work, we first predicted the landslide events of different magnitudes by quantifying a multivariate relation between landslide event-days (i.e., the day when there is a landslide event in an area) and different daily/antecedent rainfall variables because the landslides used for this work are rainfall triggered. Then, from the recurrence of such predicted events of different magnitudes, we calculated the ranges of temporal probabilities. The ranges of spatial probabilities of different landsliding events were calculated by using landslide occurrence maps of different known landsliding events and then combined with different ranges of temporal probabilities for making various landslide hazard scenarios. Finally, we calculated the number of affected elements-at-risk (e.g., buildings, population, etc.) through an exposure-based analy-

sis by incorporating each of the determined landslide hazard scenarios.

### Predicting landslide events and hazard scenarios

Landslide risk expresses the likelihood of losses arising from an event of certain magnitude within a given period of time and area (Lee and Jones 2004). Therefore, the first step of risk analysis is to characterize landslide events with varying degrees of magnitudes and determine their respective recurrence intervals. We determined the same using the event-based landslide inventory maps generated in this study area using the landslide event database of 1968–2007 (Ghosh et al. 2011b).

The temporal prediction of landslide events depends on the analysis of past event data and analysis of their return periods (RP). Due to gaps in the source data sets (e.g., 1969–1978, 1980–1992, etc.; see Table 2), the event-based landslide inventories available for the study area (Ghosh et al. 2011b), could not be used directly to calculate the return periods. Moreover, these inventories were not complete and therefore cannot provide complete information about landslide events and their varying levels of magnitudes (i.e., magnitude of events in terms of increasing number of landslide occurrences and density) that have occurred in the periods for which data is missing (Table 2). Although, the historic data gives a good indication of the importance of landslide-triggering events (e.g., landslides that occurred in 1968, 1998, 2003, etc.), still they are not exhaustive, as other triggering events might have occurred for which landslide inventories are not available (Table 2). Therefore, to model the unknown events, we established an empirical relationship between landslide events and triggering rainfall (Ghosh et al. 2011b). The landslides between 1968 and 2007 mostly occurred in the monsoon period (June–October), when precipitation is very high (between 2,500 and 3,600 mm), and accounting for 80–85% of the total annual precipitation (Soja and Starkel 2007; Starkel 2004; Starkel and Basu 2000). Therefore, we applied a stepwise discriminant analysis (DA) to establish the quantified relationship between landslide events and triggering rainfall (Ghosh et al. 2011b).

The above DA model predicted 30 landslide event-years based on a subjectively derived threshold discriminant score (DS) of 4.0 (Ghosh et al. 2011b). Based on increased DS values (along X-axis in Fig. 4) and the number of predicted landslide event-days per year (along Y-axis in Fig. 4), landslide events were classified into three classes: minor, moderate, and major events (Fig. 4), with increasing levels of magnitude. The basic assumptions we followed are that the magnitude of events will increase with increasing DS values (cf. Altman 1968; Rasmussen et al. 1985) and with the increasing number of predicted landslide event-days per event year. For example, major landslide events (e.g., LI68, LI03 in Fig. 4) have at least three landslide event-days per year and high DS values. Based on the above criteria, 16 minor, 10 moderate, and 4 major landslide events were predicted within the entire period of analysis (1968–2007). Therefore the return periods of events were assumed ranging between 3 and 5 years for minor events, 4–10 years for moderate ones, and 20–50 years for major events. These ranges of values were assumed, considering the number of occurrences of both confirmed/known and model-predicted landslide events together for the entire period of analysis (40 years, 1968–2007). The ranges of return periods or annual probabilities express the level of uncertainty in temporal probability.

**Fig. 3** Map showing major elements-at-risks of the study area. a Building density (number/100 m<sup>2</sup>), b population density (number/100 m<sup>2</sup>), and c major road networks

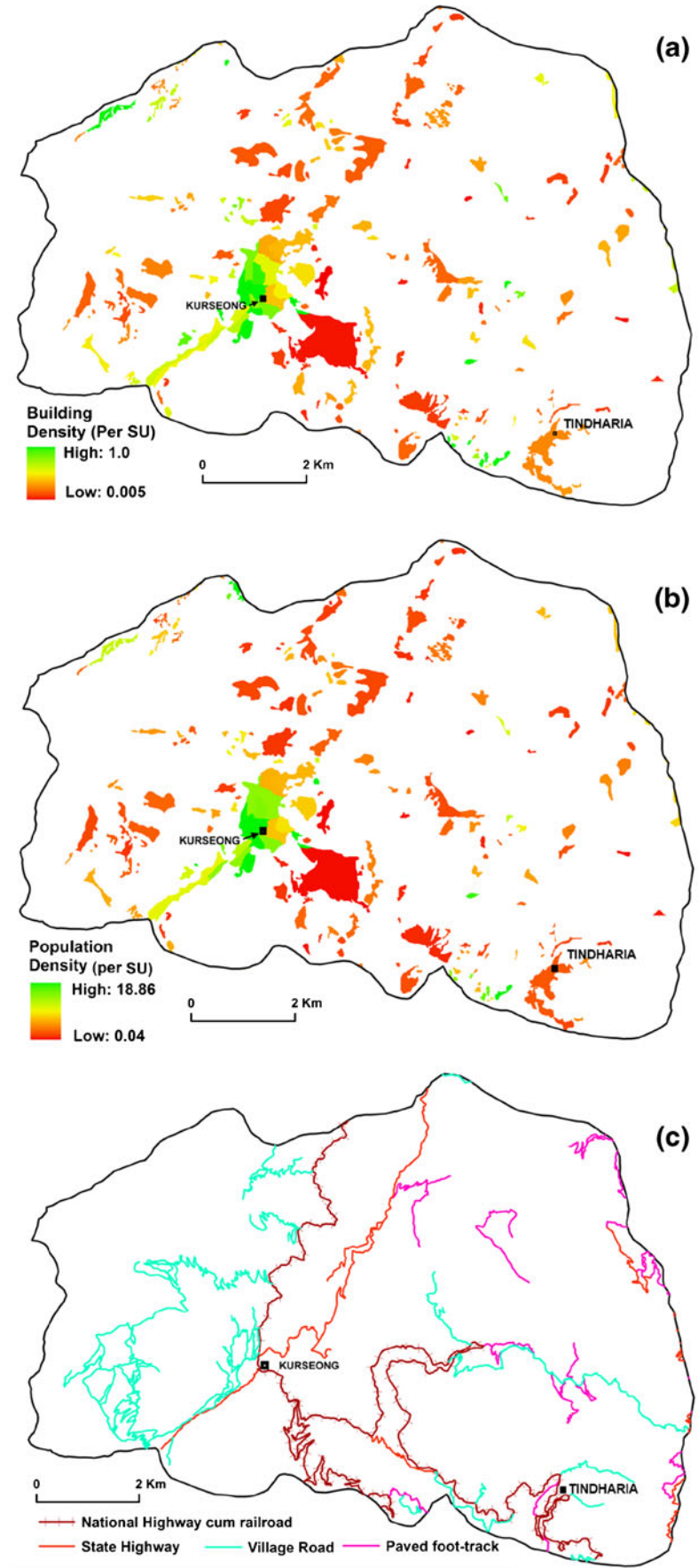


**Table 2** Types, extent, and period (date of acquisition, DOA) of source data and associated rainfall events for landslide inventory (LI)

Source data (scale/resolution)	Extent (km <sup>2</sup> )	DOA/period	Known rainfall event-days (24 days)	LI period
Topographic map (1:25,000)	90	1969–1970	2–4 October 1968	LI68
B×W stereo airphotos (1:50,000 and 1:10,000)	90	1980	12 and 24 July 1979	LI79
No source data available	90	1984	18 September 1984	–
	90	1985	18–19 October 1985	–
	90	1986	28 June 1986	–
	90	1991	9–11 September 1991	–
Field-based landslide inventory map (1:25,000)	56	1993	1–3 July 1993	LI93
Field-based landslide inventory map (1:25,000)	20	1998	6–8 July 1998	LI98
IRS 1-D PAN image (5.8 m)	90	2002	Unknown	LI99-02
IRS P-6 LISS-4 MX (5.8 m)	90	2004	5–7 July 2003	LI03
IRS P5 stereo cartosat-1 (2.5 m)	90	2006	Unknown	LI04-06
Field-based landslide inventory map (1:25,000)	90	2007	6–8 September 2007	LI07

The identification of landslide events of certain magnitudes also facilitates the correlation of predicted events with the existing landslide inventories of 1968–2007, which are required for the estimation of the spatial probability of landslides. The spatial probability ( $P_s$ ) of a pixel to have a future landslide can be calculated as:

$$P_s = L_s / S_i \quad (1)$$

where,  $L_s$  is the total landslide area in a susceptibility class  $i$ ,  $S_i$  is total area of the susceptibility class  $i$ .

The spatial probability can be calculated for different landslide magnitude scenarios indicated as major, moderate, and minor events as shown in Fig. 4. The known landslide inventories (see Table 2; Fig. 4) that are representative for the respective magnitude

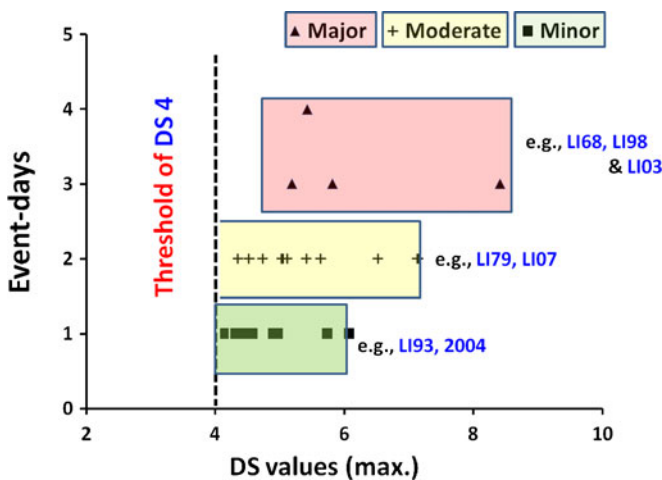


**Fig. 4** Predicted landslide events with different magnitudes. The number of landslide-triggering event-days (i.e., the day when there is a landslide event) for minor, moderate, and major events are plotted along Y-axis against the discriminant scores (DS). DS represents the discriminant scores obtained in the discriminant analysis model for each case after solving the model-derived discriminant equation. Also the known landslide inventories that matched/correlated with different magnitude classes are also shown (e.g., LI68)

classes were used to calculate the spatial probability. The variation in landslide densities per magnitude class was considered by evaluating the landslide densities of all known events that are classified in a particular magnitude class. So for instance, in case of major events, we used the landslide densities of the inventories LI68, LI98, and LI03 and the range of densities reflects the level of uncertainty in the spatial probability. Therefore, a combination of the range of temporal probabilities with the range of spatial probabilities resulted in 12 different landslide hazard scenarios that were taken into account (Fig. 5) for calculating hazard and risk.

#### Landslide risk estimation

We used 12 landslide hazard scenarios (Fig. 5) to calculate the specific risks or loss to elements-at-risks (e.g., buildings) per mapping unit (i.e., the settlement unit or SU) using an exposure-based approach, adapted from the method of rock fall hazards proposed by Lee and Jones (2004; see page 349–351). The method for calculating such loss per SU ( $L_{SU}$ ) is illustrated in Eq. 2 and in Fig. 6.

$$L_{SU} = Cell_{aff_{su}} \times P_{Cell_{occ}} \quad (2)$$

where,  $Cell_{aff_{su}} = P_s \times N_{cell_{su}}$ ;  $P_{Cell_{occ}} = N_{Elm} / N_{cell_{su}}$ ;  $Cell_{aff_{su}}$  is the number of cells affected in a SU,  $P_s$  is the spatial probability according to Eq. 1,  $N_{cell_{su}}$  is the total number of cells/pixels in a SU,  $P_{Cell_{occ}}$  is the probability of cells occupied by an elements-at-risk (e.g. buildings) in a SU and  $N_{Elm}$  is the total number of elements-at-risk (e.g., buildings) within a SU.

The first step of risk estimation is to calculate the number of cells per SU ( $Cell_{aff_{su}}$ ) that are likely to be affected by landslides given a triggering event of a certain magnitude. The  $Cell_{aff_{su}}$  is a function of the spatial probability ( $P_s$ ) that depends on the landslide susceptibility maps and also on the specific landslide distribution maps that have been identified for events of different magnitudes. The spatial probability is not calculated separately for each SU but is calculated for each class of the susceptibility map, as we assume that the landslide behavior is the same for each susceptibility class. Therefore, the proportion of cells within an SU likely to be

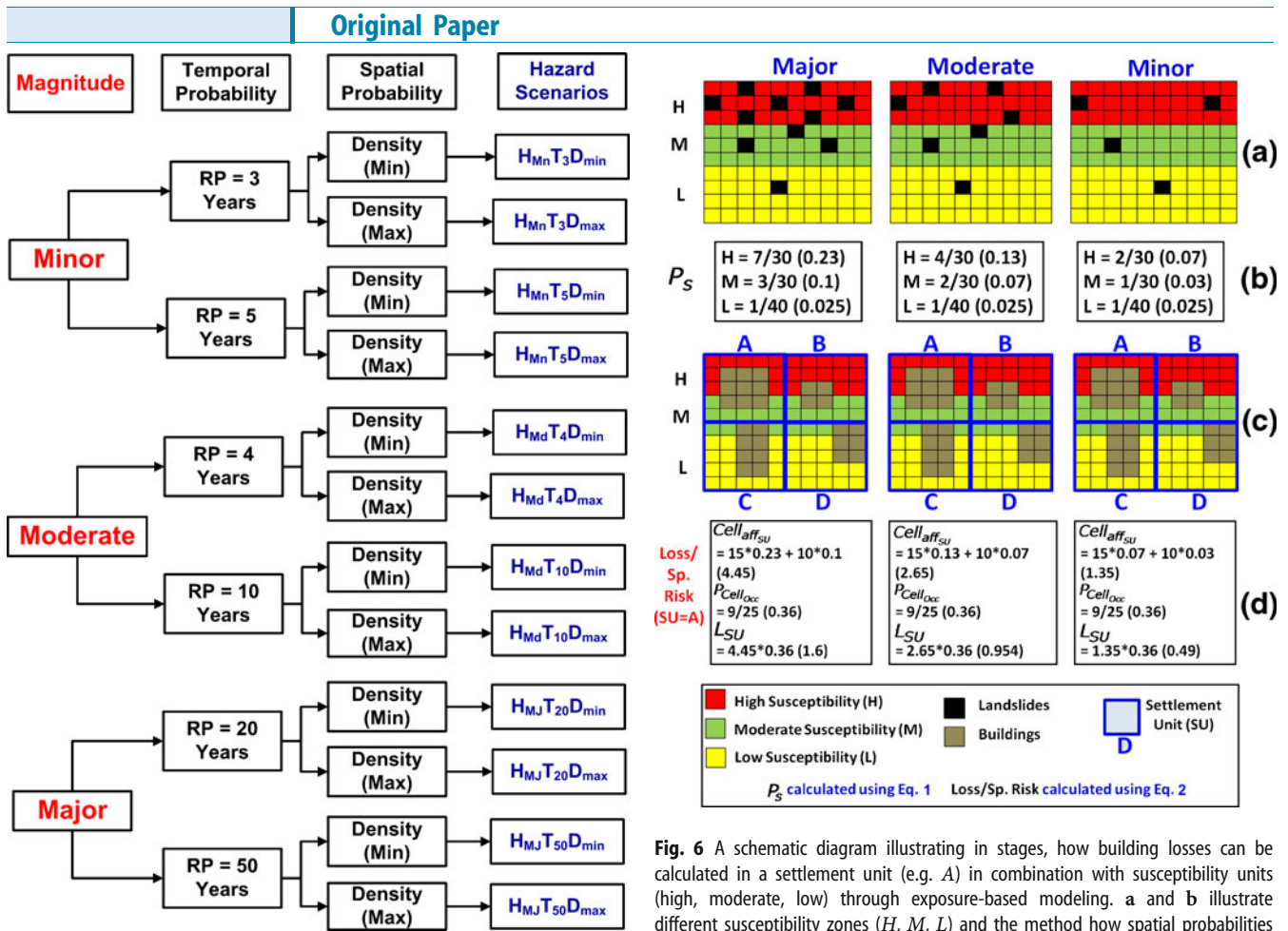


**Fig. 5** Different possible landslide hazard scenarios based on minimum and maximum temporal and spatial probabilities of landslide events of certain magnitudes. The abbreviation used for each hazard scenario (e.g.,  $H_{Mn}T_{20}D_{min}$ ) can be read as H=hazard; MJ (subscript)=major event; Md (subscript)=moderate event; Mn (subscript)=minor event; T with RP value in subscript signifies different temporal probabilities (e.g.  $T_{20}$ );  $D_{max}$  and  $D_{min}$  signifies ranges of spatial probability that has been calculated by using landslide distribution maps of maximum and minimum landslide densities respectively using Eq. 1

affected ( $Cell_{aff_{SU}}$  in Fig. 6) that actually have elements-at-risk depends on its spatial exposure with different susceptibility classes. Accordingly, we calculated the number of cells affected per settlement unit by overlaying the SU map with the susceptibility map in a GIS (Fig. 6c–d). Since a building foot print map is not available or difficult to be prepared at medium scales (1:25,000), we assumed that there is a uniform distribution of buildings within the settlement unit. Finally, the number of buildings likely to be affected can be calculated by multiplying the number of cells affected ( $Cell_{aff_{SU}}$ ) with the probability of cells occupied ( $P_{Cell_{occ}}$ ) by buildings in a settlement unit (Eq. 2 and Fig. 6c–d). It is important to mention here that we also assumed the vulnerability to the elements-at-risk to be “1”, and therefore, the results actually indicate the number of elements-at-risk likely to be affected. Given the uncertainty of the data and the medium scale of analysis, it is not possible to use vulnerability curves and express the losses as number of elements-at-risk destroyed. By adding the results for all 236 different settlement units (SU), we

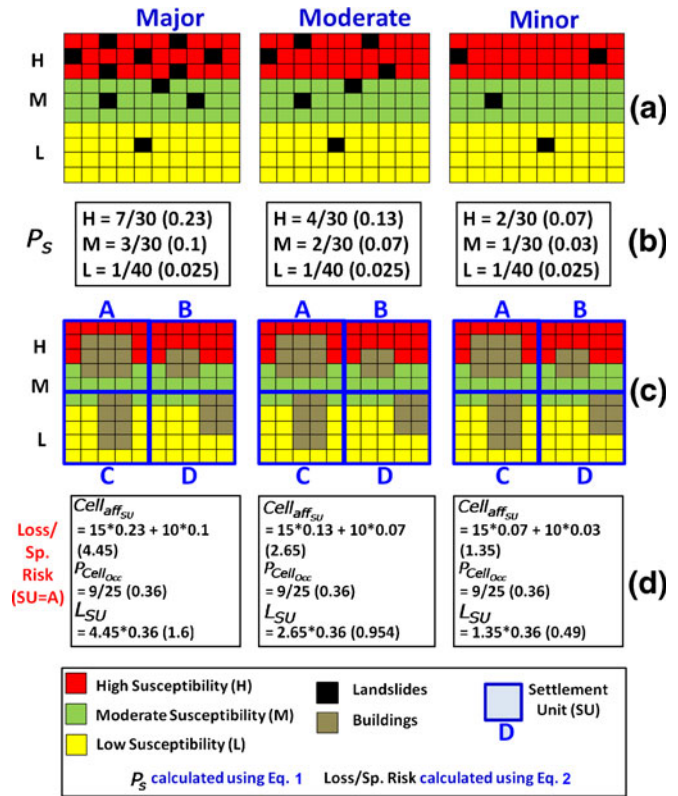


**Fig. 6** A schematic diagram illustrating in stages, how building losses can be calculated in a settlement unit (e.g. A) in combination with susceptibility units (high, moderate, low) through exposure-based modeling. a and b illustrate different susceptibility zones (H, M, L) and the method how spatial probabilities are calculated following Eq. 1 using distribution of landslides of different magnitudes (Major, Moderate, and Minor). c and d illustrate how building losses are calculated in a settlement unit (A) following Eq. 2 in three magnitude scenarios. For abbreviations at d, please refer to the explanations given in Eq. 2

calculated the total expected loss due to a particular hazard scenario and presented the corresponding losses due to the event of different magnitudes in a risk curve against the temporal probability of occurrence of the hazard scenarios. We followed the same method to calculate the expected losses to roads and population of the study area. Our inventory contains two major landslide types: rockslides and debris slides, the former being substantially more (about 70% of the total landslide population) and occurs in a discernible spatial location than the latter; we calculated the number of affected buildings, population, and roads separately for the above two landslide types.

Since the number of people living in a building during daytime and nighttime varies (about 30% of the total population) and landsliding being a discrete spatio-temporal event, the estimation of people likely to be affected should be based separately on daytime and nighttime population. We calculated the daytime population on the basis of the number of unemployed people, housewives, and small children. For the nighttime population, a proportion of 2% of the total population was excluded from the total number of inhabitants assuming that they are staying away from their homes due to some personal work. We then graphically illustrated the likely population that would be directly affected by landslides by adopting the standard frequency–number ( $F-N$ ) curves used to represent the

**Table 3** Spatial probabilities for different hazard scenarios for rockslides

Landslide event	Total pixel	Susceptibility class			
		Low 429,865	Moderate 150,612	High 158,050	Very high 155,198
Minor	$H_{Mn}D_{min}$	9.538E-05	3.785E-04	9.491E-04	1.186E-03
	$H_{Mn}D_{max}$	6.141E-04	9.827E-04	2.360E-03	2.713E-03
Moderate	$H_{Md}D_{min}$	1.605E-04	5.312E-04	7.276E-04	3.808E-03
	$H_{Md}D_{max}$	8.305E-04	3.592E-03	5.688E-03	8.815E-03
Major	$H_{Mj}D_{min}$	7.770E-04	4.289E-03	5.878E-03	1.713E-02
	$H_{Mj}D_{max}$	5.234E-04	3.214E-03	9.794E-03	5.041E-02
Extreme	$H_{Ext}$	1.117E-01	2.241E-01	2.352E-01	4.506E-01

The spatial probabilities were calculated according to Eq. 1

societal risk, in which the frequency of events ( $F$ ) that likely affect  $N$  people can be plotted along the  $Y$ -axis against the number of affected people ( $N$ ) on the  $X$ -axis on log-log scales. The frequency of events ( $N$ ) is represented by  $P_L$  which is the annual probability of the landslide event to occur, which in this case has a range with minimum and maximum values depending of landslide events of different magnitudes. The temporal spatial probability of a person or group of person based on their respective exposure in day and night time is taken into account when estimating the number of people ( $N$ ) likely to be affected, by multiplying the number of affected buildings by the average number of people per building (both during day and night time) in each settlement unit, for landslide events of different magnitudes. The vulnerability of a person or a group of persons at risk is also assumed here as 1, since the aim is only to represent the number of people likely to be affected, and not the number of people injured or killed.

We also represented the “number of likely affected buildings” and “number of affected people or likely affected population” in a map, by considering a certain period of time, instead of annualized losses. For instance, the probability that an event with a given RP is likely to occur within a 50-year period ( $T_{50}$ ) can be calculated using the following expression:

$$T_{50} = (1 - (1 - 1/RP)^{50}) \quad (3)$$

To express the number of buildings or persons affected by landslides during a period of 50-years, we can multiply  $T_{50}$  by the respective

specific losses for each return period and integrate the losses for all return periods with their respective  $T_{50}$  values. The cumulative expected losses can also be expressed annually. The annualized loss values are calculated as the “area under the risk curve”. Although, in Eq. 3, we have a simple assumption that the annual probability of occurrence of a particular landsliding event of certain magnitude will remain constant for the entire 50 years, which in practice, may not be true.

#### Results of landslide hazard estimation

Following Eq. 1, we estimated the spatial probability of landslide occurrence for the three magnitude classes (major, moderate, and minor) using both the minimum and maximum landslide density values of the known landslide inventories. This resulted in spatial probability for six different hazard scenarios and for two types of landslides (rockslides and debris slides). We presented the above results in Tables 3 (rockslides) and 4 (debris slides) for different susceptibility zones (low to very high), which are required to convert the susceptibility zones into hazard zones. Examples of specific landslide hazard maps related to major landsliding event are shown in Fig. 7, where the ranges of spatial probabilities (minimum–maximum) for each susceptibility class are shown.

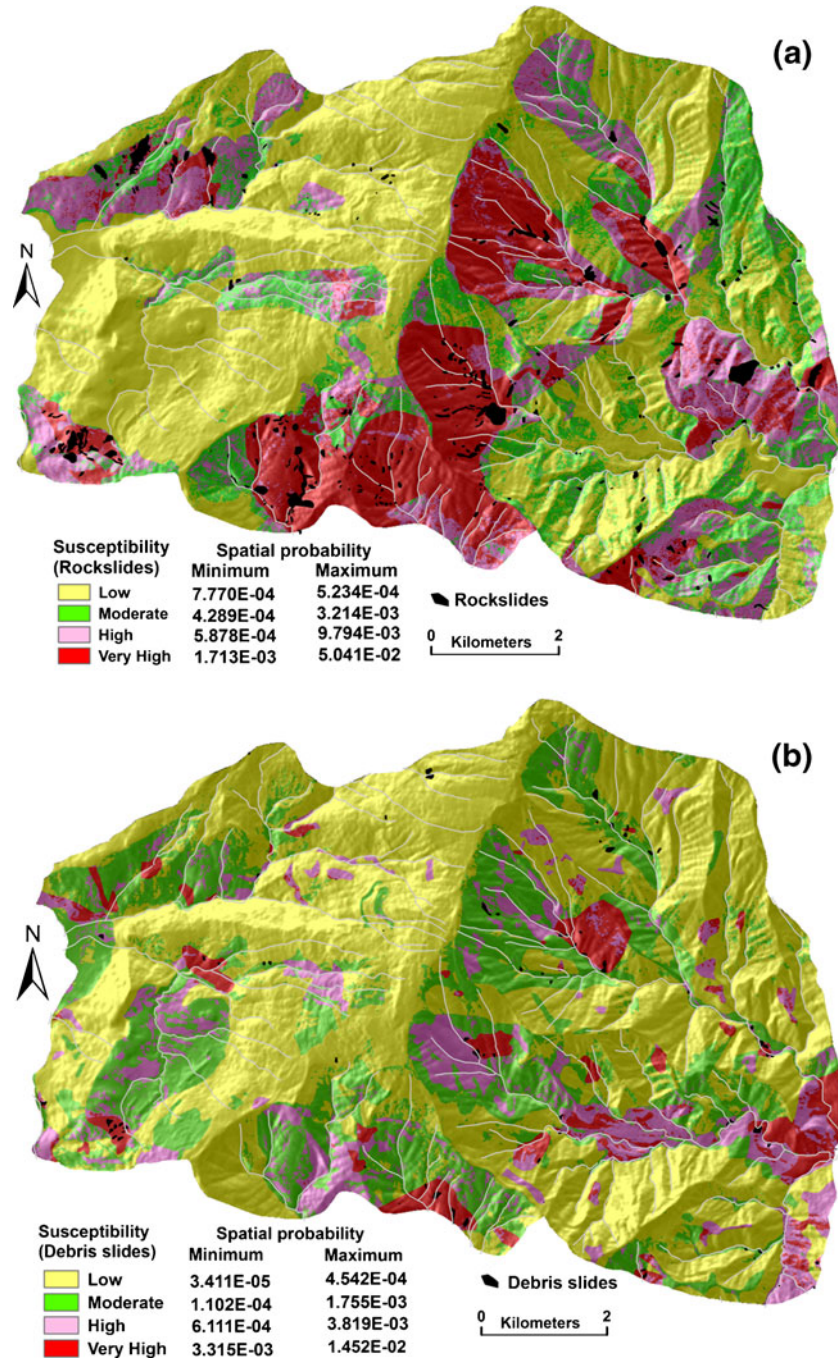
In Table 3, a hazard scenario ( $H_{Ext}$ ) has been added, which represents a hypothetical situation of an extreme landslide event caused by an earthquake occurring in the direct vicinity of the study area. Since the landslide inventories prepared from historical data since 1968 were all rainfall-triggered events, and

**Table 4** Spatial probabilities for different hazard scenarios for debris slides

Landslide event	Total pixel	Susceptibility class			
		Low 513,049	Moderate 226,781	High 104,730	Very high 49,166
Minor	$H_{Mn}D_{min}$	3.898E-05	1.980E-04	1.910E-05	2.156E-03
	$H_{Mn}D_{max}$	5.068E-05	2.999E-04	1.136E-03	5.919E-03
Moderate	$H_{Md}D_{min}$	1.169E-05	1.499E-04	9.071E-04	3.763E-03
	$H_{Md}D_{max}$	3.177E-04	7.805E-04	2.444E-03	1.277E-02
Major	$H_{Mj}D_{min}$	3.411E-04	1.102E-04	6.111E-04	3.315E-03
	$H_{Mj}D_{max}$	4.542E-04	1.755E-03	3.819E-03	1.452E-02

The spatial probabilities were calculated according to Eq. 1

**Fig. 7** Examples of landslide hazard maps showing the ranges of spatial probabilities of occurrence of landslides (see Tables 3 and 4) for major landsliding events to a rockslides and **b** debris slides in the case of a major landslide-triggering event (rainfall related)



we did not have any historical information on dates of earthquake-triggered landslides, we therefore had to make some assumptions. In the study area, there are a number of larger landslides that were already present in the first of the available landslide inventories, and that are referred to as pre-1968 (the date of the first available inventory). For calculating the spatial probability of the assumed earthquake-triggered event, the inventory of these large undated landslides of pre-1968 (see Fig. 2) was used to calculate the landslide density. The purpose of modeling such an extreme event is relevant because the study area falls within an active fold-thrust-belt of the Himalayas and is highly earthquake-prone (BIS 2002). However, data is lacking to make a more detailed analysis of return periods of earthquakes in

relation to earthquake-triggered landslide inventories. Based on expert judgment, and evaluation of earthquake catalogs and literature (Shedlock et al. 2000; Rastogi 2004; Petersen et al. 2004a, b), we assumed a range between 300 and 500 years for the return period of such an extreme scenario.

#### Expected losses to buildings and population

Based on the exposure analysis presented in Fig. 6, we calculated the ranges of buildings that are likely to be affected by minor, moderate, major, and extreme events. Depending on the variation in spatial probability due to the variation in landslide densities linked to a certain magnitude of triggering events, a range of expected loss values was analyzed. We present the results in

**Table 5** Number of buildings likely to be affected for different landslide hazard scenarios

Landslide event	Hazard scenarios	Buildings likely to be affected (rocksliding)	Buildings likely to be affected (debris sliding)	Buildings likely to be affected (total)	Temporal probability	
					Minimum AP (1/RP)	Maximum AP (1/RP)
Minor	$H_{Mn}D_{min}$	4	1	5	0.2 (1/5)	0.33 (1/3)
	$H_{Mn}D_{max}$	13	4	17		
Moderate	$H_{Md}D_{min}$	6	2	9	0.1 (1/10)	0.25 (1/4)
	$H_{Md}D_{max}$	30	10	40		
Major	$H_{Mj}D_{min}$	37	5	42	0.02 (1/50)	0.05 (1/20)
	$H_{Mj}D_{max}$	62	16	78		
Extreme	$H_{Ext}$	2,194	–	2,194	0.002 (1/500)	0.003 (1/300)

The range in temporal probability of these events is indicated  
 AP Annual probability; RP Return period in years

Table 5 showing that the number of affected buildings is generally higher for rockslides than for debris slides. In case of an extreme event the number of affected buildings is much higher (2194), compared to any of the other scenarios, due to fact that a nearby earthquake scenario can trigger many more landslides than any of the rainfall-triggered ones that occurred in the last 40 years (1968–2007).

The building losses shown in Table 5 can also be graphically represented in the form of risk curves (Fig. 8), where the variation in losses (expressed as number of buildings likely to be affected) is shown as minimum and maximum curves. The minimum risk curve is made based on the minimum values for temporal and spatial probabilities, and the maximum risk curve considers the corresponding maximum temporal and spatial probability values. The difference between the two curves is an indication of the degree of uncertainty in the risk analysis. The effect of including the extreme event is evident from Fig. 8b where the risk curves result in very different values if such an event was excluded.

The expected building losses presented in Table 5 can be directly used to calculate the number of people likely to be affected by modeling both day- and nighttime population. We present the corresponding results of the “number of affected

people or likely affected population” for different hazard scenarios in Table 6. For population living inside buildings, it is most unlikely that exposure of a person or group of persons at risk are similar for both day and night time (Table 6). The expected number of people ( $N$ ) likely to be affected for each landslide-event magnitude (see columns 7 and 8 of Table 6) are plotted in a log–log scale (Fig. 9) against the respective annual frequency ( $F$ ) of these events (columns 9 and 10 in Table 6). We do not have information on larger return periods, given the limited time period for which inventories were available; we lack information for lower frequencies. The  $F$ – $N$  curve could be used as basis for evaluating the risk acceptability level; however, there are no generally accepted risk acceptability criteria in India defined yet.

Spatially, the variability of likely losses to buildings can also be illustrated through various risk scenario maps by computing the losses based, for example on a 50-year time period (Fig. 10). Figure 10a represents the minimum losses, which have been calculated, based on minimum spatial and temporal probabilities of landsliding events. Most of the settlement units in the study area have a low range of losses (buildings affected,  $\leq 1$  per SU) with a few areas (e.g. Tindharia) having moderate losses

**Fig. 8** Loss curves showing the ranges in “the number of buildings likely to be affected” in landsliding events of different magnitudes against minimum and maximum temporal probabilities (see Table 5). The lower level loss curves in “black” represent the minimum losses plotted against minimum temporal probabilities and the upper level curves in “red” represent the maximum losses plotted against the maximum temporal probabilities. The curves at a include only major, moderate, and minor landsliding events. The curves at b include landsliding events of all magnitudes including the extreme event

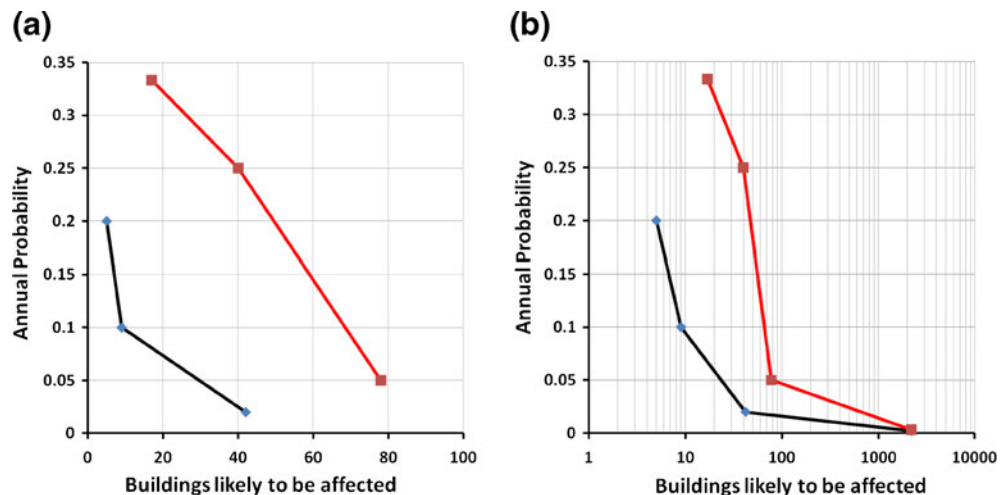


**Table 6** Values for daytime and nighttime population living in buildings likely to be affected for different landslide hazard scenarios

Landslide event	Hazard scenarios	Population likely to be affected (rocksliding)		Population likely to be affected (debris sliding)		Population likely to be affected (total)		Temporal probability	
		Day	Night	Day	Night	Day	Night	Minimum AP (1/RP)	Maximum AP (1/RP)
Minor	$H_{Mn}D_{min}$	14	21	6	9	20	30	0.2 (1/5)	0.33 (1/3)
	$H_{Mn}D_{max}$	48	70	14	22	62	92		
Moderate	$H_{Md}D_{min}$	20	32	8	13	28	45	0.1 (1/10)	0.25 (1/4)
	$H_{Md}D_{max}$	105	157	43	65	148	222		
Major	$H_{Mj}D_{min}$	124	188	24	36	148	224	0.02 (1/50)	0.05 (1/20)
	$H_{Mj}D_{max}$	183	293	66	99	249	392		
Extreme	$H_{Ext}$	7,910	11,646	–	–	7,910	11,646	0.002 (1/500)	0.003 (1/300)

AP Annual probability; RP Return period in years

(buildings affected, one to four). Figure 10b, which has been prepared based on the maximum values of spatial and temporal probabilities of landsliding events, shows that the number of settlement units having moderate losses increase substantially and the areas around Tindharia has high losses (buildings affected, four to ten). In Fig. 10c, the effects of an extreme earthquake-triggering landslide event in the vicinity has also been included. The expected losses in the Tindharia area become very high (buildings affected, ten to 15 per SU) including some parts of Kurseong municipality, which also show high losses. It is important to mention that the actual number of affected buildings in such an extreme earthquake-related scenario would be much larger due to the effects of ground shaking. In this study, only the possible effects of landslides are taken into account. The

estimation of such losses considering the 50-year time period and the annualized loss estimates for buildings and population are also shown in Table 7. This table demonstrates that the maximum annualized and 50-year losses of buildings and population increase manifold if the extreme earthquake-triggering landslide events are included. Assuming an average economic value of Indian rupees (INR) 120,000 per building (about 2,000 euros), the maximum annualized losses by landslides to buildings in the study area could range between 44,000 euros (INR 26,40,000) and 144,000 euros (INR 86,40,000) for the entire study area.

**Direct losses to major roads**

Following the above exposure-based method of loss estimation, the likely losses to the 162-km-long road network have also been estimated in the study area (Table 8). This table shows that about 893 m of the road is likely to be affected if the maximum density of a major landslide event is taken into account. Like building and population losses, length of roads (meters) likely to be affected increases about 13 times if the extreme earthquake-triggered landslide events are considered. A substantially higher proportion of the road network is affected by debris slides as compared to rock slides (Table 8) because debris slides are mostly concentrated along the major roads of the study area.

**Discussion**

This study tried to estimate landslide risk in a quantitative manner for a medium-scale analysis, by incorporating the uncertainties involved in assessing temporal, spatial, and magnitude probabilities of landslide-triggering events. Rather than calculating an average expected loss, we think it is better to express the range of expected losses given the uncertainties involved. Given the associated high uncertainties for spatial and temporal probabilities and their effect on expected losses, we feel that it is not very relevant to attempt to quantify landslide vulnerability for individual buildings at this scale of analysis, and therefore propose to use this method only to have a general estimate about the number of affected buildings and population rather than the real losses.

Due to non-availability of any proper damage records, it becomes quite difficult to properly validate the results obtained in

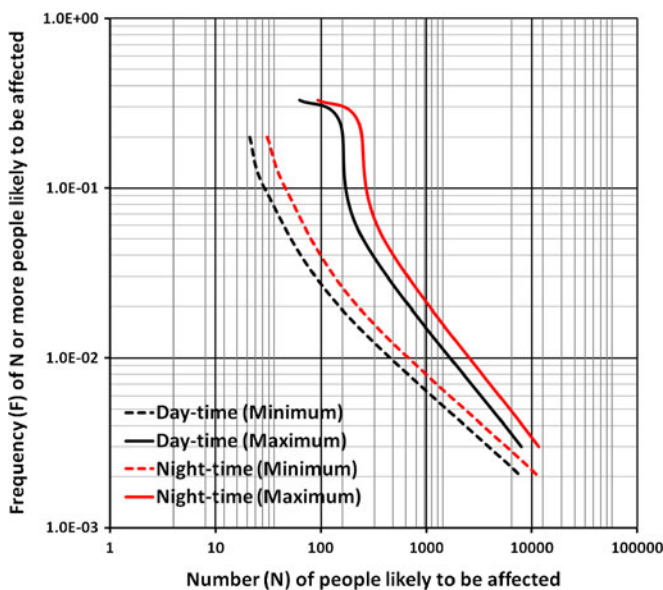


**Fig. 9** *F*–*N* curves showing annual frequency (*F*) of *N* or more people likely to be affected plotted on a log–log scale against the corresponding number of people likely to be affected for both daytime and nighttime scenarios. For each case, both “minimum” and “maximum” *F*–*N* curves are shown, which represents the minimum and maximum likely losses calculated on the basis of minimum and maximum spatial and temporal probability scenarios respectively (see Table 6)

**Fig. 10** Risk map showing spatial distribution of likely losses of affected buildings based on 50-year period due to different landslide hazard scenarios. **a** Risk map showing minimum losses based on minimum temporal and spatial probabilities; **b** risk map showing maximum losses based on maximum temporal and spatial probabilities, and **c** risk map showing extreme losses using maximum landslide density and including the probable extreme events

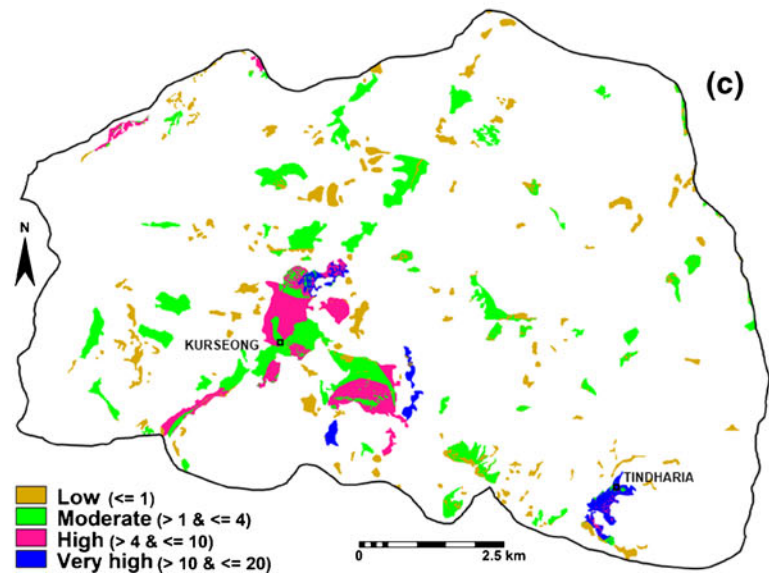
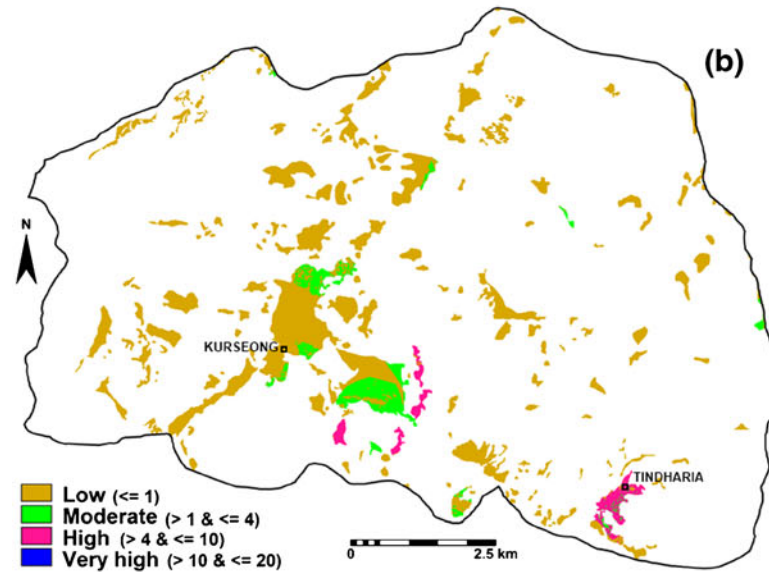
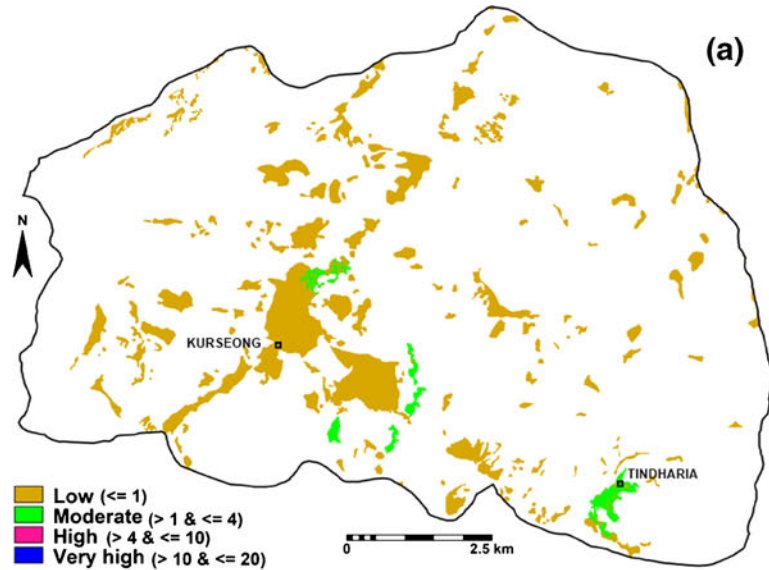


**Table 7** The annualized and 50-year loss estimates for buildings and population of the study area

Landslide events		Buildings likely to be affected				Population likely to be affected (daytime)				Population likely to be affected (nighttime)			
		Annualized		50 year		Annualized		50 year		Annualized		50 year	
		Min	Max	Min	Max	Min	Max	Min	Max	Min	Max	Min	Max
Only rainfall triggered	Rocksliding	4	17	34	100	14	56	113	323	22	85	172	497
	Debris sliding	1	5	9	35	5	20	14	57	7	30	44	179
Total		5	22	43	135	19	76	127	379	29	115	216	676
Including earthquake triggered	Rocksliding	26	72	243	438	93	253	866	1538	138	376	1281	2288

this study, although, a general indication can be obtained from reports of damage data in some recent (e.g., 1998, 2003) major landsliding events in the area. They show that during major rainfall-triggering events, a substantial portion of the road network (about 1 km) was affected causing road blockades for more than 15 days along with substantial damage to 30–40 houses in the study area (Bhattacharya et al. 1998; Paul and Sarkar 2003). This is quite in line with the calculated losses in buildings for a major event in this study (42–78) as indicated in Table 5. These landslide events can also cause indirect losses to various elements-at-risk which might be larger than the direct losses. However, it is very difficult to calculate such indirect losses, as these incorporate even more uncertainties.

Landslide risk assessment at medium-scales (1:25,000) relies primarily on the predictive mapping and landslide susceptibility estimation which remains to be the primary step in the process. The landslide susceptibility models used for this study were prepared separately for two types of landslides (rock and debris slides). Although, the risk estimation could be further improved by generating separate susceptibility maps for different landslide types for each triggering event (so separate susceptibility maps for triggering events with say 5, 10, 50, 100, and 500-year return periods) and use these in combination with their respective event-based inventories to estimate specific spatial and magnitude probabilities. We could not attempt this in the present study because of the lack of reliable and insufficient number of landslide occurrences in our available event-based landslide

inventories and also because it would make the risk models perhaps too complex given the medium-scale of assessment. It is also important to mention that despite the reasonably good quality susceptibility models (Ghosh et al. 2011a) used in this study, there are still some landslides within “low” and “moderate” susceptibility classes, which introduced some additional amount of uncertainty in the risk estimation since separate susceptibility models using only landslide occurrences of different magnitudes were not carried out due to paucity of complete landslide event–magnitude data.

The magnitude probability based on the frequency–size distributions of landslide areas ( $m^2$ ), which can be determined by fitting standard distribution functions (e.g., inverse-gamma and/or double pareto; Ghosh et al. 2011b) was not included in this study as we considered that given the high degree of uncertainty involved already and the rather general scale of analysis, the estimation of vulnerability of each elements-at-risk based on landslide sizes was not justified. However, given the availability of complete landslide inventories it could be possible to calculate the magnitude probabilities for different landslide sizes, and the same could be used to estimate the number of cells affected by larger or smaller landslides. And also, this can be used as a proxy for landslide magnitude in assigning different vulnerability values for buildings. However, as the aim of this work was to only represent the number of buildings that might be affected by landslides at a medium scale, this was considered not appropriate. Also, given the large uncertainties involved, the inclusion of more uncertain-

**Table 8** Expected direct losses to road network against the different landslide hazard scenarios

Hazard scenarios	Road (m) likely to be affected/annum due to rocksliding events	Road (m) likely to be affected/annum due to debris sliding events	Road (m) likely to be affected/annum (total)	LFE AP (1/RP)	HFE AP (1/RP)
$HZ_{Min}D_{Min}$	23	43	66	0.2 (1/5)	0.33 (1/3)
$HZ_{Min}D_{Max}$	72	121	193		
$HZ_{MD}D_{Min}$	50	77	127	0.1 (1/10)	0.25 (1/4)
$HZ_{MD}D_{Max}$	174	266	440		
$HZ_{MJ}D_{Min}$	255	75	329	0.02 (1/50)	0.05 (1/20)
$HZ_{MJ}D_{Max}$	577	316	893		
$HZ_{Ext}$	11,686	–	11,686	0.002 (1/500)	0.003 (1/300)

LFE low-frequency events, HFE high-frequency events, AP annual probability; RP return period in years

ties related to the probability of landslide sizes that would have the potential to destroy buildings, and also the vulnerability of the building themselves, were not considered justifiable.

Instead, for landslide risk assessment, modeling of different consequences is required and that is possible if the landslide-triggering events and their magnitudes are known. The determination of landslide-triggering event magnitudes is more reliable if a complete historical record of landslide events is available (Rossi et al. 2010; Salvati et al. 2010). But in most cases one has to deal with incomplete data and unavoidable gaps in landslide inventories such as in this study area. The only alternative was to establish an empirical relation between landslides and triggering events such as rainfall (Crozier 1999; Aleotti and Chowdhury 1999; Chowdhury and Flentje 2002; Jaiswal and van Westen 2009), assuming that all the landslides are rainfall triggered (Soja and Starkel 2007; Starkel 2004; Starkel and Basu 2000; Dahal and Hasegawa 2008), and that earthquake-triggered landslide events occur infrequently, but could generate many more landslides than the rainfall events. Due to non-availability of any record of such earthquake-triggered landslide events, consequence modeling in the study area was mainly based on the available record of the 40-years period (1968–2007) using only the rainfall-triggered landslides, although, this 40-year period could be quite a small period for estimating/visualizing the entire range of landslide event-magnitude scenarios. Moreover, definite data gaps even within the 40-year period of analysis made the above study more challenging that resulted in varying levels of uncertainty in loss estimation.

Due to the above data gaps, it was also difficult to characterize the landslide-event magnitude, although an arbitrary classification in minor, moderate, and major landsliding events worked well in practice in the assessment of losses. The above framework can be improved if a more complete set of historical data of landslide-event magnitudes would be available in an area, where, identification of events of different magnitudes and assessment of their respective temporal probabilities are less uncertain. However, in many cases there are simply no more historical data that could be collected, and therefore the method presented in this paper could be a useful approach to estimate the range of expected losses due to landslides in such data-scarce environments.

The risk assessment framework presented in this study is mainly aimed for the use in medium-scale risk assessment and therefore, a separate run out assessment was also not included. The currently available models for landslide runout assessment require a large number of parameters, which cannot be obtained over large areas (Kuriakose et al. 2009; Hungr and McDougall 2009; Chen and Lee 2003). Furthermore the identification of potential source areas, and more importantly, the expected initiation volumes, has such a high degree of uncertainty, that the application of such models is not practical in medium-scale landslide risk assessment (Okura et al. 2000, 2003). As discussed earlier, another simplified assumption followed in this study was not to consider the vulnerability, and therefore only estimate the number of affected elements-at-risk rather than the number of destroyed ones. This was caused due to several reasons, such as the absence of detailed building data (both building footprint data as well as building characteristics), the lack of consistent estimations of landslide magnitude parameters (Ghosh et al. 2011b) and the lack of quantitative vulnerability curves due to non-availability of any proper historic damage data, etc. The risk assessment model presented in this study is therefore a general one,

which is applicable at medium scale and mostly relies on good susceptibility maps and on event-based landslide inventories. Based on the distribution of known landslide occurrences, the ranges of uncertainty in losses for different elements-at-risk were quantitatively determined.

## Conclusions

- In a data-scarce environment, the empirical relations between triggering events (e.g., rainfall) and landslides can be used to classify the events with varying levels of magnitudes (major, moderate, and minor). Accordingly, different ranges of temporal probability can be estimated from their respective return periods.
- Using variations in the densities of known event-based landslide inventories, different landslide hazard scenarios can be generated based on minimum and maximum temporal and spatial probabilities of triggering events, which can yield different levels of annual losses to various elements-at-risk (buildings, people, road, etc.).
- This study has shown that the expected number of affected buildings annually ranges between 0.01% and 0.16% of total number of buildings (13,736), expected number of affected population ranges between 0.02% and 0.15% of the total population (76,126) and the expected section of affected roads ranges between 0.04% and 0.55% of the 162-km road lengths of the study area for landslide events of different magnitudes (minor, moderate, and major).
- The variable amounts of such losses that are shown against variable temporal and spatial probabilities can be considered as a measure of uncertainty in risk estimation in situations when there is incomplete information on historic landslides, as evident in the study area. The above results are quite plausible according to the losses occurred during similar landslide events in the recent past.
- This study also demonstrated that losses to any elements-at-risk exponentially increase if an extreme landslide event occurs in the area due to a major earthquake as evident from the hypothetical analyses of losses using pre-1968 landslides which could be assumed as earthquake triggered.

## Acknowledgements

The work presented here is part of the PhD research of Saibal Ghosh within the joint research project of the Geological Survey of India (GSI), National Remote Sensing Centre (India), ITC (The Netherlands). We are grateful to the local administrative authority of Kurseong Sub-division, Darjeeling district, Government of West Bengal, India for providing us the necessary logistics and data at field. This research was carried out in the framework of the United Nations University–ITC School for Disaster Geo-Information Management ([www.itc.nl/unu/dgim/](http://www.itc.nl/unu/dgim/)).

## References

- Aleotti P, Chowdhury R (1999) Landslide hazard assessment: summary review and new perspectives. *Bull Eng Geol Environ* 58:21–44
- Altman E (1968) Financial ratios, discriminant analysis and the prediction of corporate bankruptcy. *J Finance* 23(4):189–209

- Anbalagan R, Singh B (1996) Landslide hazard and risk assessment mapping of mountainous terrains—a case study from Kumaun Himalaya, India. *Eng Geol* 43(4):237–246
- Bhattacharya A, Mishra P, Ghoshal TB, Bahuguna H, Ghatak T (1998) A geotechnical appraisal of landslides on 7th July, 1998 along National Highway No. 55. In: GSI (ed) Progress report (F.S. 1998–99)
- Binnie SA, Phillips WM, Summerfield MA, Fifield LK (2007) Tectonic uplift, threshold hillslopes and denudation rates in developing mountain range. *Geology* 35:743–746
- BIS (2002) Criteria for earthquake resistant design of structures: general provisions and buildings, Bureau of Indian Standards (BIS) IS 1893:2002 (Part-1)
- Burbank DW, Leland J, Fielding E, Anderson RS, Brozovic N, Reid MR, Duncan C (1996) Bedrock incision, rock uplift and threshold hillslopes in the northwestern Himalayas. *Nature* 379:505–510
- Caine N, Mool PK (1982) Landslides in the Kolpu Khola drainage, Middle Mountains, Nepal. *Mt Res Dev* 2(2):157–173
- Chen H, Lee CF (2003) A dynamic model for rainfall-induced landslides on natural slopes. *Geomorphology* 51(4):269–288
- Chowdhury R, Flentje P (2002) Uncertainties in rainfall-induced landslide hazard. *Q J Eng Geol Hydrogeol* 35:61–70
- Crozier MJ (1999) Prediction of rainfall-triggered landslide: a test of antecedent water status model. *Earth Surface Processes and Landforms* 24:825–833
- Cruden DM (1997) Estimating the risk from landslides using historical data. In: Cruden D, Fell R (eds) Landslide risk assessment. A.A. Balkema, Rotterdam, pp 177–184
- Dahal RK, Hasegawa S (2008) Representative rainfall thresholds for landslides in the Nepal Himalaya. *Geomorphology* 100(3–4):429–443
- Dutta KK (1966) Landslips in Darjeeling and neighbouring hill-slopes in June, 1950. In: GSI (ed) Landslides and Hillside stability in the Eastern Himalayas, vol 15. Geological Survey of India Bulletin Series B Kolkata, pp 7–30
- Einstein HH (1997) Landslide risk—systematic approaches to assessment and management. In: Cruden D, Fell R (eds) Landslide risk assessment. A.A. Balkema, Rotterdam, pp 25–50
- Fell R, Hartford D (1997) Landslide risk management. In: Cruden D, Fell R (eds) Landslide risk assessment. A.A. Balkema, Rotterdam, pp 51–109
- Fell R, Corominas J, Bonnard C, Cascini L, Leroi E, Savage WZ (2008) Guidelines for landslide susceptibility, hazard and risk zoning for land use planning. *Eng Geol* 102(3–4):85–98
- Ghosh S, Carranza EJM (2010) Spatial analysis of mutual fault/fracture and slope controls on rocksliding in Darjeeling Himalaya, India. *Geomorphology* 122(1–2):1–24
- Ghosh S, Carranza EJM, van Westen CJ, Jetten VG, Bhattacharya DN (2011a) Selecting and weighting of spatial predictors for empirical modeling of landslide susceptibility in Darjeeling Himalaya (India). *Geomorphology*. doi:10.1016/j.geomorph.2011.04.019
- Ghosh S, van Westen CJ, Carranza EJM, Jetten VG, Cardinali M, Rossi M, Guzzetti F (2011b) Generating event-based landslide maps in a data-scarce Himalayan environment for estimating temporal and magnitude probabilities. *Engineering Geol*. doi:10.1016/j.enggeo.2011.03.016
- Guzzetti F (2002) Landslide hazard assessment and risk evaluation: overview, limits and perspective. In: 3rd MITCH workshop floods, droughts and landslides: who plans, who pays, Potsdam, Germany, 24–26 November 2002
- Guzzetti F, Carrara A, Cardinali M, Reichenbach P (1999) Landslide hazard evaluation: a review of current techniques and their application in a multi-scale study, Central Italy. *Geomorphology* 31(1–4):181–216
- Guzzetti F, Reichenbach P, Cardinali M, Galli M, Ardizzone F (2005) Probabilistic landslide hazard assessment at the basin scale. *Geomorphology* 72(1–4):272–299
- Hungr O, McDougall S (2009) Two numerical models for landslide dynamic analysis. *Comput Geosci* 35(5):978–992
- Jaiswal P, van Westen CJ (2009) Estimating temporal probability for landslide initiation along transportation routes based on rainfall thresholds. *Geomorphology* 112(1–2):96–105
- Kanungo D, Arora M, Gupta R, Sarkar S (2008) Landslide risk assessment using concepts of danger pixels and fuzzy set theory in Darjeeling Himalayas. *Landslides* 5(4):407–416
- Kuriakose SL, van Beek LPH, van Westen CJ (2009) Parameterizing a physically based shallow landslide model in a data poor region. *Earth Surface Processes and Landforms* 34(6):867–881. doi:10.1002/esp.1794
- Lee EM, Jones DKC (2004) Landslide risk assessment, 1st edn. ThomasTelford, London
- Malamud BD, Turcotte DL, Guzzetti F, Reichenbach P (2004) Landslide inventories and their statistical properties. *Earth Surface Processes and Landforms* 29(6):687–711
- Okura Y, Kitahara H, Sammori T, Kawanami A (2000) The effects of rockfall volume on runout distance. *Eng Geol* 58(2):109–124
- Okura Y, Kitahara H, Kawanami A, Kurokawa U (2003) Topography and volume effects on travel distance of surface failure. *Eng Geol* 67(3–4):243–254
- Paul C, Sarkar NK (2003) A note on the recent landslide damage assessment along different road stretches in Darjeeling Hills, West Bengal (as an aftermath of July 2003 deluge). In: GSI (ed) Progress report (F.S. 2003–04)
- Petersen MD, Dewey J, Hartzell S, Mueller C, Harmsen S, Frankel A, Rukstales K (2004a) Probabilistic seismic hazard analysis for Sumatra, Indonesia and across the Southern Malaysian Peninsula. *Tectonophysics* 390(1–4):141–158
- Petersen MD, Rastogi BK, Schweig ES, Harmsen SC, Gombert JS (2004b) Sensitivity analysis of seismic hazard for the northwestern portion of the state of Gujarat, India. *Tectonophysics* 390(1–4):105–115
- Petley D, Hearn G, Hart A, Rosser N, Dunning S, Oven K, Mitchell W (2007) Trends in landslide occurrence in Nepal. *Nat Hazard* 43(1):23–44
- Rasmussen HH, Pitt EA, Ibel LS, McNeil DR (1985) Prediction of outcome in acute renal failure by discriminant analysis of clinical variables. *Arch Intern Med* 145(11):2015–2018
- Rastogi BK (2004) Damage due to the Mw7.7 Kutch, India earthquake of 2001. *Tectonophysics* 390(1–4):85–103
- Rautela P, Lakhera RC (2000) Landslide risk analysis between Giri and Tons Rivers in Himachal Himalaya (India). *Int J Appl Earth Obs Geoinform* 2(3–4):153–160
- Rossi M, Witt A, Guzzetti F, Malamud BD, Peruccacci S (2010) Analysis of historical landslide time series in the Emilia-Romagna region, northern Italy. *Earth Surface Processes and Landforms* 35(10):1123–1137. doi:10.1002/esp.1858
- Salvati P, Bianchi C, Rossi M, Guzzetti F (2010) Societal landslide and flood risk in Italy. *Nat Hazards Earth Syst Sci* 10(3):465–483. doi:10.5194/nhess-10-465-2010
- Selby MJ (1988) Landforms and denudation of the High Himalayas of Nepal: results of continental collision. *J Geomorphol, New Folge* 69: 133–152, Supplementebande
- Shedlock KM, Giardini D, Grunthal G, Zhang P (2000) The GSHAP global seismic hazard map. *Seismol Res Lett* 71(6):679–686. doi:10.1785/gssrl.71.6.679
- Soja R, Starkel L (2007) Extreme rainfalls in Eastern Himalaya and southern slope of Meghalaya Plateau and their geomorphologic impacts. *Geomorphology* 84(3–4):170–180
- Starkel L (2004) Extreme rainfall at 5–7 July 1998 in the Darjeeling Himalaya. In: Sing S, Sharma HS, De SK (eds) *Geomorphology and environment*. ABC Publications, Kolkata, pp 26–31
- Starkel L, Basu S (2000) Rains, landslides and floods in the Darjeeling Himalaya. Indian National Science Academy, New Delhi
- van Westen CJ, van Asch TWJ, Soeters R (2006) Landslide hazard and risk zonation—why is it still so difficult? *Bull Eng Geol Environ* 65(5):167–184
- Varnes DJ (1984) Landslide hazard zonation: a review of principles and practice. UNESCO, Darantiere
- Zêzere JL, Garcia RAC, Oliveira SC, Reis E (2008) Probabilistic landslide risk analysis considering direct costs in the area north of Lisbon (Portugal). *Geomorphology* 94(3–4):467–495

### S. Ghosh

Engineering Geology Division, Geological Survey of India, Eastern Region, Kolkata, India

### S. Ghosh (✉) · C. J. van Westen · E. J. M. Carranza · V. G. Jetten

Department of Earth System Analysis, Faculty of Geo-Information Science and Earth Observation (ITC), University of Twente, Enschede, The Netherlands  
e-mail: ghosh@itc.nl